Research Article | Vol. 30, No. 21 / 10 Oct 2022 / Optics Express 37888
Optics EXPRESS

Communication wavelength investigation of bound states in the continuum of one-dimensional two-material periodic ring optical waveguide network

YAN ZHI,[1] WEICI LIU,[2] XIANGBO YANG,[1] ZHONGCHAO WEI,[1] SHIPING DU,[2] HONGYUN MENG,[1] HONGZHAN LIU,[1] JIANPING GUO,[1] MANXING YANG,[1] JIANAN WANG,[1] LIUJING XIANG,[1] ZHENMING HUANG,[1] HAOXIAN LI,[1] AND FAQIANG WANG[1,*]

[1]*Guangzhou Key Laboratory for Special Fiber Photonic Devices, Laboratory of Nanophotonic Functional Materials and Devices, School of Information and Optoelectronic Science and Engineering, South China Normal University, Guangzhou 510006, China*
[2]*School of Engineering, Guangzhou College of Technology and Business, Foshan 528138, China*
[*]*fqwang@scnu.edu.cn*

Abstract: In this study, a one-dimensional (1D) two-material period ring optical waveguide network (TMPROWN) was designed, and its optical properties were investigated. The key characteristics observed in the 1D TMPROWN include the following: (1) Bound states in continuum (BICs) can be generated in the optical waveguide network. (2) In contrast to the BICs previously reported in optical structures, the range of the BICs generated by the 1D TMPROWN is not only larger, but also continuous. This feature makes it possible for us to further study the electromagnetic wave characteristics in the range of the BICs. In addition, we analyzed the physical mechanisms of the BICs generated in the 1D TMPROWN. The 1D TMPROWN is simple in structure, demonstrates flexibility with respect to adjusting the frequency band of the BICs, and offers easy measurement of the amplitude and phase of electromagnetic waves. Hence, further research on high-power super luminescent diodes, optical switches, efficient photonic energy storage, and other optical devices based on the 1D TMPROWN designed in this study is likely to have implications in a broad range of applications.

1. Introduction

Since the introduction of bound states in continuum (BICs) [1] by Neumann and Wigner in 1929, it has been widely applied in the fields of quantum mechanics, acoustics, water waves, and optics [2–17]. The typical characteristics of BICs include: (1) Electromagnetic (EM) wave lies in continuum. (2) EM wave should be radiated but remains bounded in special optical structure [2]. BICs are found in a wide variety of material systems through a binding mechanism that is completely different from the traditional bound state [2]. In recent years, since photonic structures can be tailored in terms of their materials and structures, the unique properties of BICs in optical structures have led to the development of several devices, such as filters, low-loss fibers, lasers, and sensors.

Notably, BICs are primarily classified into two types: symmetrical protection and resonance-trapped BICs [2]. Ideal BICs exist only in lossless structures [6,18] or at extreme parameter values [7,11]. In general, resonance-trapped BICs can be realized via inverse construction in optical metasurfaces, waveguide structures, and photonic crystals [8–12]. However, since the inherent non-radiative property of ideal BICs is the disappearance of the resonance linewidth, BICs cannot be observed in the electromagnetic spectrum. Consequently, optical structures in

#471602 https://doi.org/10.1364/OE.471602
Journal © 2022 Received 4 Aug 2022; revised 10 Sep 2022; accepted 17 Sep 2022; published 28 Sep 2022

Optics EXPRESS

practical applications are frequently designed using quasi-BICs [7,13–17], and optical properties in the range of BICs have not been studied.

Optical waveguide networks (OWNs) have been extensively studied over the last two decades and have been widely used to observe related optical phenomena, such as photonic localization [19,20], non-reciprocity of EM wave propagation [20,21,22,23,24], Bloch oscillation [25,26], Rabi oscillation [27], slow light effect [28] and ultrastrong extraordinary transmission and reflection characteristics [29–31]. Additionally, they can form an artificial photonic bandgap (PBG) structure that can limit and control the propagation of EM waves [25–28,32–44] and can produce ultrawide PBG [41]. Besides, the structural connection of the OWN is extremely flexible, and the flexible connection between the waveguide segments makes it easier to realize a rich symmetry and high-dimensional structures [32,33].

The prerequisite of investigating the properties of BICs in a special optical structure requires that the BICs generated must be nonzero line-width, and this case does not studied in the past literatures. Instantaneously, because most wave systems prohibit BICs in compact structures, so lots of theoretically proposed or experimentally observed BICs are implemented as extended optical structures. Therefore, in general, structures yielding BICs extend to infinity in at least one direction [2]. Under the conditions of the optical structure based on previous design, we design a 1D TMPROWN composed of lithium chloride (LiCl) which can saturate the condition of nonzero line-width.

In this study, we search for BICs in OWN systems in regards to ultrawide PBG and superior optical properties of the OWN system and explore the properties of the BICs generated in the OWN. Actually, the distribution range of the BICs is determined by adjusting the structural parameters of the 1D TMPROWN and calculating the photon mode and transmission. Subsequently, the mechanism of BIC generation is explained by calculating the distribution of the photonic localization in the waveguide segment. Since the amplitude and phase of the EM wave propagating through the OWN can be easily measured at each node, we anticipate the discovery of novel characteristics of BICs that are not found in other optical systems, which can serve as a solid foundation for the practical application of BICs.

This paper is organized as follows. Section 2 introduces the model and theory. In Section 3, we explain the causes of the formation of the BICs and investigate the unique optical properties of the 1D TMPROWN in the range of the BICs. Finally, the conclusions of this study are presented in Section 4.

2. Model and theory

2.1. 1D TMPROWN

A schematic of the 1D TMPROWN is shown in Fig. 1, where the length of each waveguide segment is denoted by d. We ensure that the regions where not only obvious BICs can be generated, but also it is with extremely weak LiCl dispersion are located near the communication wavelength by repeatedly adjusting the length parameter d. Finally, we set $d = 131\mu m$. Let l_1 and l_2 represent the length ratios in this study, and $l_1 = l_2$. In Fig. 1, the blue solid lines at the entrance and exit represent the optical waveguide segments in vacuum with a refractive index of $n_0 = 1$. The red solid lines in the unit cells represent the two-material optical waveguide segments composed of LiCl, whose refractive indices for the two sub-waveguides are:

$$\begin{cases} n_1 = n_{\mathrm{LiCl}} + n_b, \\ n_2 = n_{\mathrm{LiCl}}, \end{cases} \tag{1}$$

where n_{b} and n_{LiCl} are of the same order of magnitude, and n_{b} is an adjustable parameter of refractive index.

Optics EXPRESS

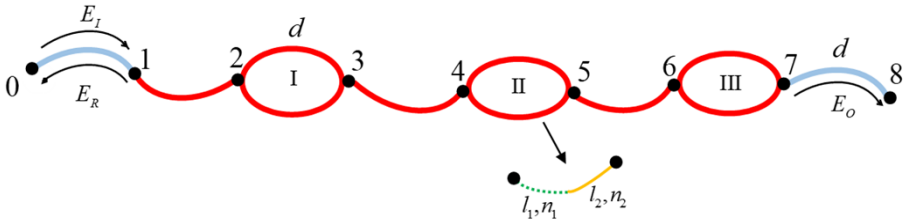

Fig. 1. Schematic of the 1D TMPROWN. A component of 1D TMPROWN consists of three unit cells (each of which is represented by a single solid red line and red ring), an entrance, and exit, where E_I, E_R, and E_O represent the input, reflective, and output EM waves, respectively. Each waveguide segment is of length d. The solid blue lines represent the optical vacuum waveguide segments at the entrance and exit. The solid red lines in the unit cells represent the two-material optical waveguide segments with refractive indices of n_1 and n_2 and length ratios of l_1 and l_2.

It is reported that in the frequency range 18.73–1763.48 THz (i.e., 0.17–16.00 μm), the dispersion relation for LiCl satisfies the following equation: [45]

$$n_{\mathrm{LiCl}}^2 - 1 = 1.51 + \frac{0.24\lambda^2}{\lambda^2 - 0.137^2} + \frac{9.11\lambda^2}{\lambda^2 - 49.26^2}, \tag{2}$$

The corresponding dispersion curve for LiCl is illustrated in Fig. 2.

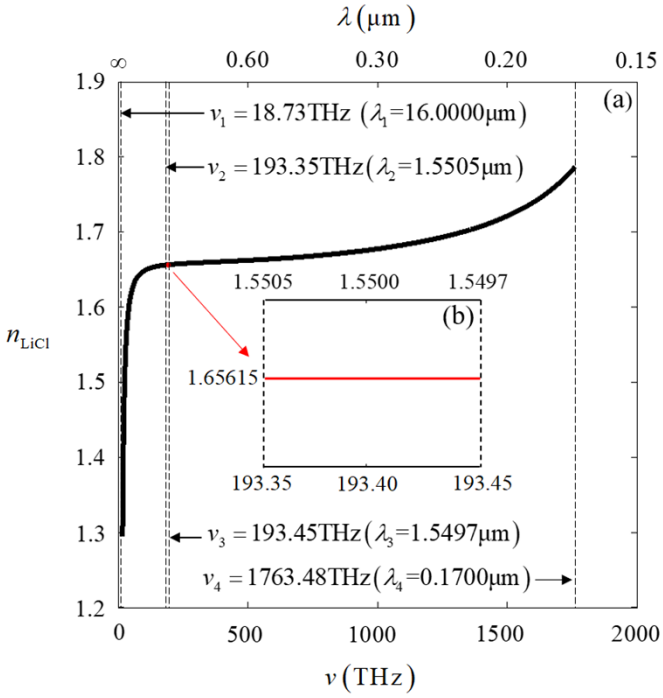

Fig. 2. Dispersion curve of LiCl. (a) A total view in the range 18.73–1763.48 THz (0.1700 –16.0000 μm). (b) An enlarged view in the range 193.35–193.45 THz (1.5497-1.5505 μm).

It can be observed from Fig. 2 (a) that LiCl exhibits a low dispersion in the frequency range 193.35–1763.45 THz (0.1700–1.5505 μm). Thus, to inhibit the effect of workload and dispersion

Optics EXPRESS

on the results and to investigate the photonic characteristics in the range of the BICs near the communication wavelength, we only use EM waves with frequencies (wavelengths) between 193.35–193.45 THz (1.5497–1.5505 μm), which correspond to the dispersion curve of the red solid line in Fig. 2 (b).

2.2. Generalized eigenfunction method and generalized Floquet–Bloch theorem

In this study, the generalized eigenfunction method [46] is used to calculate the transmissivity, reflectivity, and photonic localization, and the generalized Floquet–Bloch theorem [33] is used to obtain the dispersion relation and determine the distribution of photonic modes. The generalized Floquet-Bloch theorem is expressed as follows:

$$\psi_{\boldsymbol{K}}(\boldsymbol{N}+\boldsymbol{T}) = \psi_{\boldsymbol{K}}(\boldsymbol{N})e^{\iota \boldsymbol{K}\cdot\boldsymbol{T}}, \tag{3}$$

where $\boldsymbol{K}$, $\boldsymbol{N}$, and $\boldsymbol{T}$ denote the structure Bloch wave vector, node scaling vector, and structure translation vector, respectively.

2.3. Two-material network equation

The wave equation of the EM wave in a two-material network can be expressed as: [47]

$$\frac{\partial^2}{\partial x^2}\psi_{n_m}(x) + k_m^2\psi_{n_m}(x) = 0, \tag{4}$$

where ν is the EM wave frequency, k_m is the wave vector of magnitude $2\pi\nu n_m/\mathrm{c}$ ($m = 0,\ 1,\ 2$), and c is the speed of the EM wave in vacuum. For the 1D waveguide segments in TMPROWN, we only consider the mono-mode propagation of EM waves. Thus, the wave function between two adjacent nodes i and j can be represented as:

$$\psi_{ij}(x) = \begin{cases} \psi_{n_1}(x) = a_1 e^{\iota k_1 x} + b_1 e^{-\iota k_1 x} (0 \le x \le l_1 d_{ij}), \\ \psi_{n_2}(x) = a_2 e^{\iota k_2 x} + b_2 e^{-\iota k_2 x} (l_1 d_{ij} \le x \le d_{ij}). \end{cases} \tag{5}$$

At $x = l_1 d_{ij}$, using the continuity of the wave function and its differential quotient, we obtain:

$$\begin{cases} a_1 e^{\iota k_1 l_1 d_{ij}} + b_1 e^{-\iota k_1 l_1 d_{ij}} = a_2 e^{\iota k_2 l_1 d_{ij}} + b_2 e^{-\iota k_2 l_1 d_{ij}}, \\ a_1 k_1 e^{\iota k_1 l_1 d_{ij}} - b_1 k_1 e^{-\iota k_1 l_1 d_{ij}} = a_2 k_2 e^{\iota k_2 l_1 d_{ij}} - b_2 k_2 e^{-\iota k_2 l_1 d_{ij}}. \end{cases} \tag{6}$$

Using Eqs. (5) and (6), we obtain:

$$\psi_{ij}(x) = \begin{cases} \psi_{n_1}(x) = \dfrac{A_1 a_2 e^{\iota k_2 l_1 d_{ij}} + A_2 b_2 e^{-\iota k_2 l_1 d_{ij}}}{2k_1 e^{\iota k_1 l_1 d_{ij}}} e^{\iota k_1 x} \\ \qquad\qquad + \dfrac{A_2 a_2 e^{\iota k_2 l_1 d_{ij}} + A_1 b_2 e^{-\iota k_2 l_1 d_{ij}}}{2k_1 e^{-\iota k_1 l_1 d_{ij}}} e^{-\iota k_1 x} (0 \le x \le l_1 d_{ij}), \\ \psi_{n_2}(x) = a_2 e^{\iota k_2 x} + b_2 e^{-\iota k_2 x} (l_1 d_{ij} \le x \le l_{12} d_{ij}), \end{cases} \tag{7}$$

where

$$\begin{cases} A_1 = k_1 + k_2, \\ A_2 = k_1 - k_2. \end{cases} \tag{8}$$

Let ψ_i and ψ_j be the wave functions at nodes i and j, respectively. Using the continuity of the wave functions, we obtain:

$$\begin{cases} \psi_{ij}(x)|_{x=0} = \psi_i, \\ \psi_{ij}(x)|_{x=d_{ij}} = \psi_j. \end{cases} \tag{9}$$

Optics EXPRESS

Using Eqs. (7)–(9), we obtain:

$$\begin{cases} \frac{1}{2k_1}(a_2+b_2)(A_1\cos D_2 + A_2\cos D_1) \\ +\frac{\iota}{2k_1}(a_2-b_2)(A_1\sin D_2 + A_2\sin D_1) = \psi_i, \\ (a_2+b_2)\cos k_2 d_{ij} + \iota(a_2-b_2)\sin k_2 d_{ij} = \psi_j, \end{cases} \tag{10}$$

where

$$\begin{cases} D_1 = k_2 l_1 d_{ij} + k_1 l_1 d_{ij}, \\ D_2 = k_2 l_1 d_{ij} - k_1 l_1 d_{ij}. \end{cases} \tag{11}$$

Using Eqs. (7), (8), (10), and (11) yields:

$$\begin{cases} \psi_{n_1}(x) = \frac{[A_1\cos(D_2+k_1x)+A_2\cos(D_1-k_1x)]}{2k_1}\frac{[\psi_i 2k_1\sin k_2 d_{ij}-\psi_j(A_1\sin D_2+A_2\sin D_1)]}{A_1\sin D_3+A_2\sin D_4} \\ \quad + \frac{[A_1\sin(D_2+k_1x)+A_2\sin(D_1-k_1x)]}{2k_1}\frac{[\psi_j(A_1\cos D_2+A_2\cos D_1)-\psi_i 2k_1\cos k_2 d_{ij}]}{A_1\sin D_3+A_2\sin D_4} \\ (0 \le x \le l_1 d_{ij}), \\ \psi_{n_2}(x) = \frac{\psi_i 2k_1\sin k_2 d_{ij}-\psi_j(A_1\sin D_2+A_2\sin D_1)}{A_1\sin D_3+A_2\sin D_4}\cos k_2 x \\ \quad + \frac{\psi_j(A_1\cos D_2+A_2\cos D_1)-\psi_i 2k_1\cos k_2 d_{ij}}{A_1\sin D_3+A_2\sin D_4}\sin k_2 x \\ (l_1 d_{ij} \le x \le d_{ij}), \end{cases} \tag{12}$$

where

$$\begin{cases} D_3 = k_2 l_2 d_{ij} + k_1 l_1 d_{ij}, \\ D_4 = k_2 l_2 d_{ij} - k_1 l_1 d_{ij}. \end{cases} \tag{13}$$

Owing to the energy flux conservation, for any node, we have,

$$\sum_j \frac{1}{\mu\omega} A_{ij}\psi_{ij}(x)\frac{\partial\psi_{ij}(x)}{\partial x}|_{x=0} = 0, \tag{14}$$

where the summation is over all the segments directly linked to node i. Since the cross-sectional areas A_{ij} of all segments are identical, the boundary conditions in Eqs. (9) and (14) yield the following equation:

$$\sum_j \frac{\partial\psi_{ij}(x)}{\partial x}|_{x=0} = 0. \tag{15}$$

Thus, we can obtain the following updated two-material network equation with a multiconnected network [48] by applying Eqs. (7), (8), (12) and (13) to Eq. (15):

$$\begin{aligned} &-\psi_i k_1 \sum_j \frac{A_1\cos D_3 - A_2\cos D_4}{A_1\sin D_3+A_2\sin D_4} - \psi_i \sum_j \frac{2k_1 k_2\cos k_2 d_{ij}}{A_1\sin D_3+A_2\sin D_4} \\ &+ \sum_j \psi_j \frac{2k_1 k_2}{A_1\sin D_3+A_2\sin D_4} + \sum_j \psi_j k_2 \frac{A_1\cos D_2+A_2\cos D_1}{A_1\sin D_3+A_2\sin D_4} = 0. \end{aligned} \tag{16}$$

3. Results and discussions

3.1. Photonic modes

The photonic mode can be classified into three categories based on the topological translational periodicity of the EM wave propagating through the optical waveguide network: (I) when the

Optics EXPRESS

structural Bloch vector K lies in the range of real number, the photonic mode corresponds to the ordinary propagation mode (OPM) [49]. (II) when the structural Bloch vector K is in the range of complex numbers and $K = K_{\mathrm{I}} + \iota K_{\mathrm{II}}$ ($K_{\mathrm{II}} > 0$), the photonic mode corresponds to the attenuation propagation mode (AMP) [20]. (III) when the structural Bloch vector K is in the range of complex numbers and $K = K_{\mathrm{I}} + \iota K_{\mathrm{II}}$ ($K_{\mathrm{II}} < 0$), the photonic mode corresponds to the gain propagation mode (GPM) [20].

We obtain the following dispersion relation for 1D TMPROWN with infinite unit cells based on the generalized Floquet–Bloch theorem and two-material network equation:

$$\cos K = f(\nu), \tag{17}$$

where

$$f(\nu) = \frac{9(k_1 G_2 + k_2 G_1)^2 - 5(k_1 G_4 + k_2 G_3)^2}{4(k_1 G_4 + k_2 G_3)}, \tag{18}$$

and

$$\begin{cases} G_1 = \frac{2k_1 \cos k_2 d_{ij}}{A_1 \sin D_3 + A_2 \sin D_4}, \\ G_2 = \frac{A_1 \cos D_3 - A_2 \cos D_4}{A_1 \sin D_3 + A_2 \sin D_4}, \\ G_3 = \frac{A_1 \cos D_2 + A_2 \cos D_1}{A_1 \sin D_3 + A_2 \sin D_4}, \\ G_4 = \frac{2k_2}{A_1 \sin D_3 + A_2 \sin D_4}. \end{cases} \tag{19}$$

Since the refractive indices of the vacuum and/or the dielectric waveguides are real, the dispersion function $f(\nu)$ of the 1D two-material ring OWN must be real. A real $f(\nu)$ includes two cases: (I) If $|f(\nu)| \leq 1$, then K is in the range of real numbers. EM waves in this frequency range propagate as OPM and form passbands, and a large transmission is generated. The transmissivity T in this case generally satisfies the relation $0.01 \leq T \leq 1$ and does not decrease with the increase in the number of unit cells [20,33,49]. (II) If $|f(\nu)| > 1$, then K is in the range of complex numbers, EM waves in this frequency range propagate as APM, EM waves in materials without gain mechanism propagate only as APM and form PBG. Hence, a small transmission, generally satisfying the relation $T < 0.01$, is produced, and the transmissivity decreases with the increase in the number of unit cells [20,33,49].

The refractive index of the two materials used in the 1D TMPROWN is a real number. From Eqs. (18) and (19), we obtain the dispersion equation $f(\nu)$ for the entire frequency range. From Eq. (17), we can deduce that the structural Bloch wave vector K has both real and complex solutions for $f(\nu)$. In two-material networks, EM waves propagate mathematically as OPM and APM. Because of the lack of a **gain mechanism** in the 1D TMPROWN, EM waves propagate as OPM and APM.

3.2. Bound states in the continuum

To determine the BICs generated by the 1D TMPROWN designed in our study, we use the generalized eigenfunction method and generalized Floquet–Bloch theorem to calculate the transmissivity and photonic mode in the total frequency range illustrated in Fig. 2 (b). The results are shown in Fig. 3.

Figure 3(a) demonstrates that for the 1D TMPROWN, the red and blue areas represent the three distinct types of Bloch photonic modes, the OPM and APM, respectively, which are classified by the corresponding structural Bloch wave vectors. In Fig. 3 (b), the three green solid lines labeled 1, 2, and 3 denote the boundaries of the two distinct photonic modes. The transmission coefficient of the white region is greater than or equal to 0.01; the transmission coefficient of the white-grid region is less than 0.01.

In general, when an EM wave propagates as an OPM in a 1D TMPROWN, the transmission typically equals or exceeds 0.01. When an EM wave propagates as an APM, the transmissivity

Optics EXPRESS

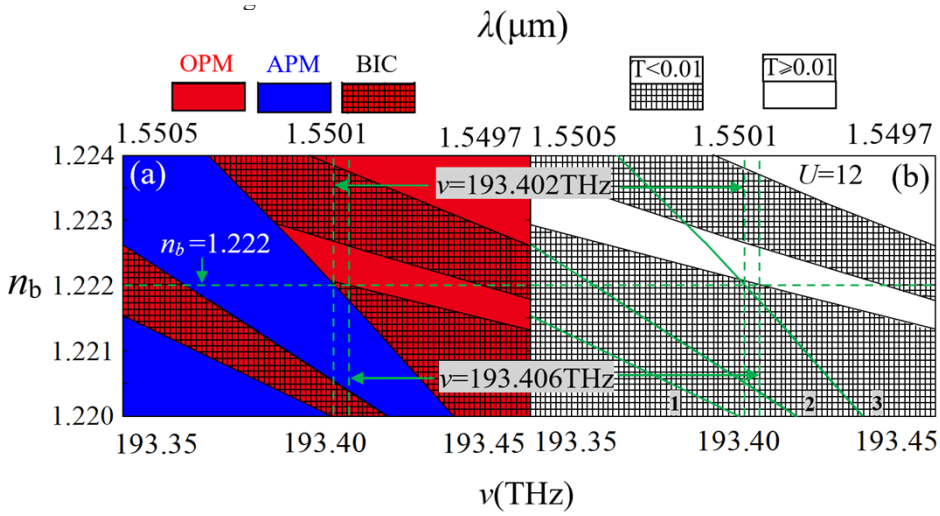

Fig. 3. Spectrum structures of the left incident EM wave propagating in the 1D TMPROWN near the communication wavelength. (a) Photonic modes distribution diagram. (b) Two-dimensional transmission spectra of the 1D TMPROWN with twelve unit cells between the frequency (horizontal ordinate) and n_b (vertical ordinate). Three green solid lines labeled 1, 2, and 3 denote the boundaries of the two distinct photonic modes. Label conventions: There are five legends above the graph, from the left to right, they are OPM, APM, BIC, T < 0.01, and T≥0.01, labelled with red color, blue color, red-grid, white-grid, and white color, respectively.

is typically less than 0.01. However, in the red-grid region in Fig. 3 (a), the transmissivity of the EM waves propagating as an OPM is less than 0.01. At this point, the red-grid area may be the PBG zone. To confirm the preceding conclusion, we calculated the transmission of the EM waves for systems of different sizes in the black-grid region. Considering the red-grid area near the communication wavelength in Fig. 3 (a) as an example, Fig. 4 shows the transmission when $n_b = 1.222$.

As shown in Fig. 4, the transmission of the system decreased exponentially as the number of unit cells increased. Consequently, we can assert that the PBG is formed in the red-grid area. Usually, in the continuous domain, the BIC domain is a special state, nevertheless it is local [2]. Therefore, we can conclude that the region where the EM wave propagates as the OPM and is in the PBG is the distribution range of the BICs, such as the red-grid area in Fig. 3 (a). This is the first key characteristic observed in the 1D TMPROWN.

To further investigate the physical mechanism of the BICs generated by the 1D TMPROWN, we calculated the distribution of the photonic localization of the 1D TMPROWN with three unit cells using the BICs range near the communication wavelength as an example. The results are shown in Fig. 5.

As can be seen in Fig. 5, the photons in each waveguide segment of the 1D TMPROWN with three unit cells are localized in the waveguide in the form of a standing-wave-like, and the photonic localization at the node and middle of each waveguide segment is significantly small, which can be considered as a wave node. The results in Fig. 5 demonstrate that the BICs generated in the OPM region are created by the standing-wave-like effect caused by the propagation of the EM wave in the 1D TMPROWN.

It is accepted that BICs can be generated in a 1D TMPROWN because each waveguide segment is composed of two segments that can lead to the formation of a sudden refractive

Optics EXPRESS

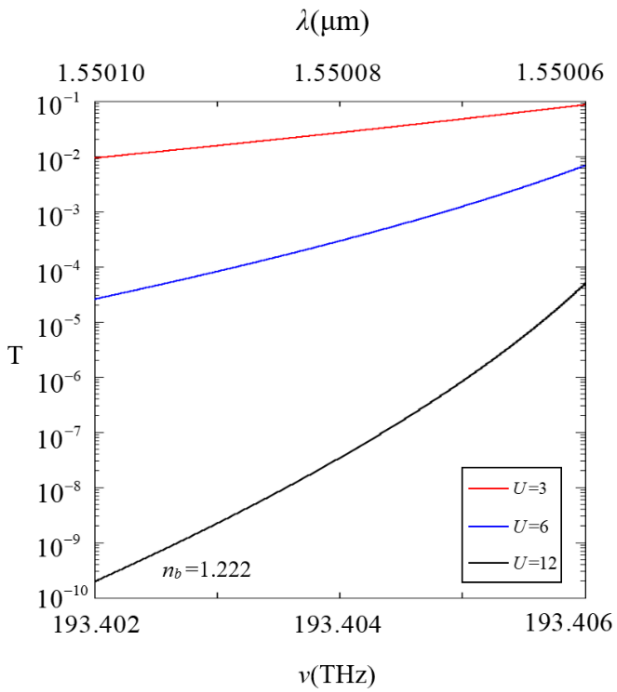

Fig. 4. The transmission spectra of the left incident EM wave propagating in the 1D TMPROWN in the range of the black-grid area near the communication wavelength, with red, blue, and black solid lines representing the transmission for unit cell counts of 3, 6, and 12, respectively.

index gradient, causing EM waves in certain ranges of the OPM to generate a standing-wave-like pattern when propagating in the 1D TMPROWN. The following section explains the reason why a 1D TMPROWN can produce a range of BICs that are not only larger, but also continuous. Each unit cell in the 1D TMPROWN consists of a waveguide segment and ring. However, the waveguide segment and ring are two distinct coupling resonant cavities. In addition, the alternating arrangement of the waveguide segments and rings enhances the resonant effect of the photonic coupling. Therefore, when EM waves propagate in the 1D TMPROWN, they complete complex coherent superposition several times, which further strengthens the standing-wave-like pattern and finally results in multiple continuous BICs.

Optics EXPRESS

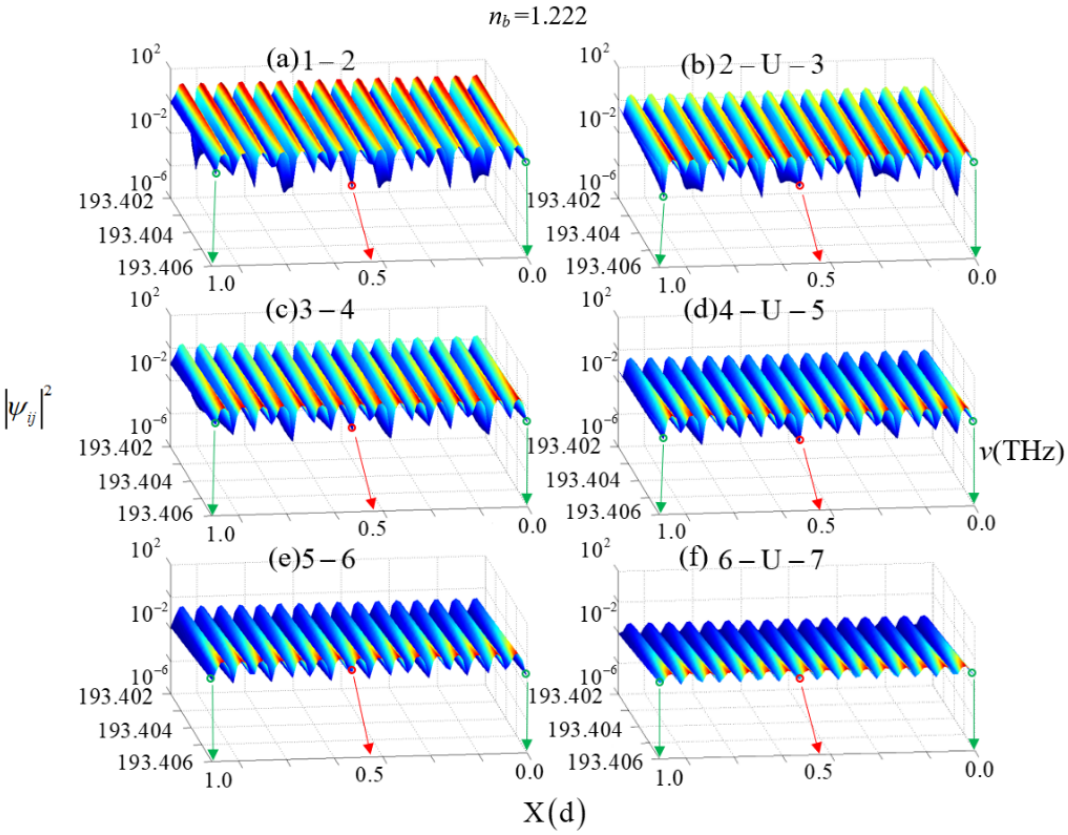

Fig. 5. Three-dimensional photonic localization intensity map of the BICs in the 1D TMPROWN with three unit cells. (a), (c), and (e): The distribution of the photonic localization for the three waveguide segments between the nodes 1 and 2, 3 and 4, and 5 and 6, respectively. (b), (d), and (f): The distribution of the photonic localization of the upper or lower arm between the nodes 2 and 3, 4 and 5, and 6 and 7, respectively. The green circle represents the node of the waveguide segment, while the red circle represents the midpoint.

4. Conclusions

In this study, we designed a 1D TMPROWN composed of LiCl to investigate the BICs generated by EM waves propagating in OWN. The following key characteristics were observed in the course of the study: (I) A large range of continuous BICs generated in the network is observed. We can flexibly adjust the distribution range and frequency of the BICs by regulating the refractive index of the materials, refractive index difference, and waveguide line length and thus analyze the mechanism of the BICs caused by a standing-wave-like effect. (II) We have also observed that the photons in the range of BICs produce strong localization owing to the standing-wave-like effect. There are standing wave nodes at the nodes and in the middle of the waveguide segments. This is because the refractive index between the adjacent waveguide segments and that between the sub-waveguides are different. Therefore, phase mutation and formation of a wave node occur when an EM wave propagates at the junction of adjacent waveguide segments and two sub-waveguides. BICs in an appropriate frequency-band range can be selected because the proposed TMPROWN has a simple structure and can flexibly be adjusted the value of n_b to meet practical needs. Additionally, the amplitude and phase of the EM wave propagating through the OWN can be easily measured at each node. Therefore, the 1D TMPROWN has potential

Optics EXPRESS

implications in the design of all-optical devices. Considering many advantages of the 1D TMPROWN, we believe that 1D TMPROWN may have potential and wide application value following further in-depth research.

Funding. Key Project of DEGP (2022KTSCX166); National Natural Science Foundation of China (11674109, 61774062, 62175070).

Disclosures. The authors declare no conflicts of interest.

Data availability. The data underlying the results presented in this paper are not publicly available at this time but may be obtained from the authors upon reasonable request.

References

1. J. von Neuman and E. Wigner, "Über merkwürdige diskrete eigenwerte," Phys. Z. **30**, 465–467 (1929).
2. C. W. Hsu, B. Zhen, A. D. Stone, J. D. Joannopoulos, and M. Soljacić, "Bound states in the continuum," Nat. Rev. Mater. **1**(9), 16048–16061 (2016).
3. B. Zhen, C. W. Hsu, L. Lu, A. D. Stone, and M. Soljačić, "Topological nature of optical bound states in the continuum," Phys. Rev. Lett. **113**(25), 257401 (2014).
4. K. Koshelev and Y. Kivshar, "Light trapping gets a boost," Nature **574**(7779), 491–492 (2019).
5. M. Minkov, D. Gerace, and S. Fan, "Doubly resonant $\chi(2)$ nonlinear photonic crystal cavity based on a bound state in the continuum," Optica **6**(8), 1039–1045 (2019).
6. N. A. Cumpsty and D. S. Whitehead, "The excitation of acoustic resonances by vortex shedding," J. Sound Vib **18**(3), 353–369 (1971).
7. J. Q. Niu, Y. Q. Zhai, Q. Q. Han, J. Q. Liu, and B. Yang, "Resonance-trapped bound states in the continuum in metallic THz metasurfaces," Opt. Lett. **46**(2), 162–165 (2021).
8. S. Campione, S. Liu, L. I. Basilio, L. K. Warne, W. L. Langston, T. S. Luk, J. R. Wendt, J. L. Reno, G. A. Keeler, I. Brener, and M. B. Sinclair, "Broken symmetry dielectric resonators for high quality factor Fano metasurfaces," ACS Photonics **3**(12), 2362–2367 (2016).
9. W. X. Liu, Y. Sun, Z.Q. Lai, and H. Chen, "Sharp optical magnetic resonances in dielectric waveguide grating structures," J. Opt. Soc. Am. B **34**(9), 1899–1904 (2017).
10. A. Taghizadeh and I. S. Chung, "Quasi bound states in the continuum with few unit cells of photonic crystal slab," Appl. Phys. Lett. **111**(3), 031114 (2017).
11. B. Midya and V. V. Konotop, "Coherent-perfect-absorber and laser for bound states in a continuum," Opt. Lett. **43**(3), 607–610 (2018).
12. L. L. Doskolovich, E. A. Bezus, and D. A. Bykov, "Integrated flat-top reflection filters operating near bound states in the continuum," Photonics Res. **7**(11), 1314–1322 (2019).
13. M. C. Panmai, J. Xiang, S. L. Li, X. B. He, Y. H. Ren, M. X. Zeng, J. C. She, J. T. Li, and S. Lan, "High efficient nonlinear optical emission from a subwavelength crystalline silicon cuboid mediated by supercavity mode," Nat. Commun. **13**(1), 2749 (2022).
14. L. Foglia, F. Capotondi, R. Mincigrucci, D. Naumenko, E. Pedersoli, A. Simoncig, G. Kurdi, A. Calvi, M. Manfredda, L. Raimondi, N. Mahne, M. Zangrando, C. Masciovecchio, and F. Bencivenga, "First Evidence of Purely Extreme-Ultraviolet Four-Wave Mixing," Phys. Rev. Lett. **120**(26), 263901 (2018).
15. J. F. Algorri, F. D. Olio, P. Roldán-Varona, L. RodrÍguez-Cobo, J. M. López-Higuera, J. M. Sanchez-Pena, and D. C. Zografopoulos, "Strongly resonant silicon slot metasurfaces with symmetry-protected bound states in the continuum," Opt. Express **29**(7), 10374–10385 (2021).
16. J. N. Wang, W. C. Liu, Z. C. Wei, H. Y. Meng, H. Z. Liu, J. P. Gou, M. X. Yang, Y. K. Song, L. J. Xiang, and Z. M. Huang, "A Bifunctional Silicon Dielectric Metasurface Based on Quasi-bound States in the Continuum," Nanomaterials **11**(9), 2357 (2021).
17. D. J. Liu, F. Wu, R. Yang, L. Chen, X. Y. He, and F. Liu, "Quasi-bound states in the continuum in metal complementary periodic cross-shaped resonators at terahertz frequencies," Opt. Lett. **46**(17), 4370–4373 (2021).
18. R. Parker, "Resonance effects in wake shedding from parallel plates: some experimental observations," J. Sound Vib **4**(1), 62–72 (1966).
19. S. A. Dyakov, M. V. Stepikhova, A. A. Bogdanov, A. V. Novikov, D. V. Yurasov, M. V. Shaleev, Z. F. Krasilnik, S. G. Tikhodeev, and N. A. Gippius, "Photonic Bound States in the Continuum in Si Structures with the Self-Assembled Ge Nanoislands," Laser Photonics Rev. **15**(7), 2000242 (2021).
20. Y. Zhi, X. B. Yang, J. Y. Wu, S. P. Du, P. C. Cao, D. C. Cao, D. M. Deng, and C. T. Liu, "Extraordinary characteristics for one-dimensional parity-time-symmetric periodic ring optical waveguide networks," Photonics Res. **6**(6), 578–586 (2018).
21. Z. Lin, H. Ramezani, T. Eichelkraut, T. Kottos, H. Cao, and D. N. Christodoulides, "Unidirectional invisibility induced by T-symmetric periodic structures," Phys. Rev. Lett. **106**(21), 213901 (2011).
22. L. Ge, Y. D. Chong, and A. D. Stone, "Conservation relations and anisotropic transmission resonances in one-dimensional PT-symmetric photonic heterostructures," Phys. Rev. A **85**(2), 023802 (2012).

Optics EXPRESS

23. Y. Choi, C. Hahn, J. W. Yoon, S. H. Song, and P. Berini, "Extremely broadband, on-chip optical nonreciprocity enabled by mimicking nonlinear anti-adiabatic quantum jumps near exceptional points," Nat. Commun. **8**(14154), 1–9 (2017).
24. Y. Zhang, X. B. Yang, F. Tang, X. M. Wang, D. M. Deng, H. Z. Liu, and Z. C. Wei, "Singular systematic phases, transparencies, and invisibilities produced by parity-time-symmetric Thue–Morse optical waveguide networks," Results Phys. **30**(104763), 1–18 (2021).
25. R. Morandotti, U. Peschel, J. S. Aitchison, H. S. Eisenberg, and Y. Silberberg, "Experimental Observation of Linear and Nonlinear Optical Bloch Oscillations," Phys. Rev. Lett. **83**(23), 4756–4759 (1999).
26. T. Pertsch, P. Dannberg, W. Elflein, A. Bräuer, and F. Lederer, "Optical Bloch Oscillations in Temperature Tuned Waveguide Arrays," Phys. Rev. Lett. **83**(23), 4752–4755 (1999).
27. K. Shandarova, C. E. Ruter, D. Kip, K. G. Makris, D. N. Christodoulides, O. Peleg, and M. Segev, "Experimental Observation of Rabi Oscillations in Photonic Lattices," Phys. Rev. Lett. **102**(12), 123905 (2009).
28. A. Nandy and A. Chakrabarti, "Engineering slow light and mode crossover in a fractal-kagome waveguide network," Phys. Rev. A **93**(1), 013807 (2016).
29. J. Y. Wu and X. B. Yang, "Ultrastrong extraordinary transmission and reflection in PT-symmetric Thue-Morse optical waveguide networks," Opt. Express **25**(22), 27724–27735 (2017).
30. J. Y. Wu, X. H. Wu, X. B. Yang, and H. Y. Li, "Extraordinary transmission and reflection in PT -symmetric two-segment-connected triangular optical waveguide networks with perfect and broken integer waveguide length ratios*," Chin. Phys. B **28**(10), 104208 (2019).
31. H. Y. Li, X. B. Yang, J. Y. Wu, and X. H. Wu, "Extraordinary characteristics of one-dimensional *PT* -symmetric ring optical waveguide networks with near-isometric and isometric arms," EPL **131**(5), 54001 (2020).
32. Z. Q. Zhang, C. C. Wong, K. K. Fung, Y. L. Ho, W. L. Chan, S. C. Kan, T. L. Chan, and N. Cheung, "Observation of localized electromagnetic waves in three-dimensional networks of waveguides," Phys. Rev. Lett. **81**(25), 5540–5543 (1998).
33. Z. Y. Wang and X. B. Yang, "Strong attenuation within the photonic band gaps of multiconnected networks," Phys. Rev. B **76**(23), 235104 (2007).
34. L. Dobrzynski, A. Akjouj, B. Djafari-Rouhani, J. O. Vasseur, and J. Zemmouri, "Giant gaps in photonic band structures," Phys. Rev. B **57**(16), R9388–R9391 (1998).
35. J. O. Vasseur, B. Djafari-Rouhani, L. Dobrzynski, A. Akjouj, and J. Zemmouri, "Defect modes in one-dimensional comblike photonic waveguides," Phys. Rev. B **59**(20), 13446–13452 (1999).
36. M. H. Li, Y. Y. Liu, and Z. Q. Zhang, "Photonic band structure of Sierpinski waveguide networks," Phys. Rev. B **61**(23), 16193–16200 (2000).
37. S. K. Cheung, T. L. Chan, Z. Q. Zhang, and C. T. Chan, "Large photonic band gaps in certain periodic and quasiperiodic networks in two and three dimensions," Phys. Rev. B **70**(12), 125104 (2004).
38. B. Pal, P. Patra, J. P. Saha, and A. Chakrabarti, "Engineering wave localization in a fractal waveguide network," Phys. Rev. A **87**(2), 023814 (2013).
39. W. Zheng, X. B. Yang, D. M. Deng, and H. Z. Liu, "Singular properties generated by finite periodic PT-symmetric optical waveguide network," Opt. Express **27**(2), 1538–1552 (2019).
40. J. Zheng, X. B. Yang, X. Zhang, D. M. Deng, and H. Z. Liu, "Transmission characteristics of one-dimensional periodic optical waveguide networks," Phys. Rev. A **99**(2), 023809 (2019).
41. X. H. Xu, J. Lu, and X. B. Yang, "Ultrawide photonic band gaps with the limit of gap-midgap ratio of 200% produced from complete-connected networks," Opt. Express **29**(14), 21576–21585 (2021).
42. J. Y. Wu and X. B. Yang, "Theoretical Design of a Pump-Free Ultrahigh Efficiency All-Optical Switching Based on a Defect Ring Optical Waveguide Network," Ann. Phys. **531**(2), 1800258 (2019).
43. X. R. Yao, X. B. Yang, Q. Wang, M. Zhang, D. M. Deng, H. Z. Liu, and Z. C. Wei, "Characteristics and mechanism of all-optical switching based on a one-dimensional two-connected periodic triangle optical waveguide network," Appl. Opt. **59**(27), 8182–8189 (2020).
44. M. Zhang, X. B. Yang, Q. Wang, X. R. Yao, D. M. Deng, H. Z. Liu, and Z. C. Wei, "Characteristics and mechanism of all-optical switching based on one-dimensional periodic two-segment-connected tetrahedral optical waveguide network," Opt. Commun. **474**, 126091 (2020).
45. H. H. Li, "Refractive index of alkali halides and its wavelength and temperature derivatives," J. Phys. Chem. **5**(2), 329–528 (1976).
46. Y. Y. Liu, Z. L. Hou, P. M. Hui, and W. Sritrakool, "Electronic transport properties of Sierpinski lattices," Phys. Rev. B **60**(19), 13444–13452 (1999).
47. Z. Q. Zhang and P. Sheng, "Wave localization in random networks," Phys. Rev. B **49**(1), 83–89 (1994).
48. Y. Wang, X. B. Yang, J. Lu, G. G. Zhang, and T. C. Liu, "Comb-like optical transmission spectra generated from one-dimensional two-segment connected two-material waveguide networks optimized by genetic algorithm," Phys. Lett. A **378**(16-17), 1200–1207 (2014).
49. X. H. Xu, X. B. Yang, S. Q. Wang, T. C. Liu, and D. M. Deng, "Sufficient condition for producing photonic band gaps in one-dimensional optical waveguide networks," Opt. Express **23**(21), 27576–27588 (2015).